Journal of Applied Polymer Science

Online Ultrasonic Film Casting of LLDPE and LLDPE/Clay Nanocomposites

Setareh Niknezhad, Avraam I. Isayev
Department of Polymer Engineering, the University of Akron, Akron, Ohio 44325-0301
Correspondence to: A. I. Isayev (E-mail: aisayev@uakron.edu)

ABSTRACT: Transparent cast films of linear low density polyethylene (LLDPE) with nanoclay up to 10 wt % were prepared in one step process using an ultrasonically assisted compounding extruder operating at various ultrasonic amplitudes combined with film casting machine operating at various take up speeds. Thermal, rheological, morphological, and mechanical properties and gas permeability of these films were studied. Ultrasonic treatment introduced an increase in the complex viscosity and storage modulus and a reduction in the tangent loss of LLDPE/clay nanocomposite melts. Cast films prepared by ultrasonic treatment at an amplitude of 7.5 μm showed the highest mechanical properties in both the machine and transverse directions and the lowest oxygen permeability. X-ray diffraction patterns along with the SEM and TEM images revealed the presence of the exfoliated structure due to the ultrasonic treatment for cast films containing up to 7.5 wt % of clay loading. NMR studies of LLDPE cast films showed an increase of branching due to the ultrasound treatment. © 2012 Wiley Periodicals, Inc. J. Appl. Polym. Sci. 129: 263–275, 2013

KEYWORDS: films; polyolefins; clay; nanostructured polymers; rheology

Received 30 July 2012; accepted 15 October 2012; published online 6 November 2012
DOI: 10.1002/app.38725

INTRODUCTION

Polyethylene (PE) is one of the most widely used polyolefins because of its attractive combination of a low production cost, low density, acceptable heat distortion temperature, chemical inertness, and easy processability. PE does not have any polar group in its backbone. Hence, dispersion of nanoclay containing the hydrophilic silicate layers in this matrix without using suitable compatibilizers is a challenging problem. Modified silicates layered with alkylammonium makes the hydrophilic silicate surface organophilic. This modification of nanoclays is one of the solutions to achieve intercalated morphology in PE nanocomposites.

Among various applications of PE, packaging is one of the most important applications for PE. The two most commonly used methods in preparation of packaging films are film blowing and film casting. Both methods need a good control of processing conditions to prepare films with good properties. PE is used in the film industry for food packaging, agricultural film, and garbage bags. LLDPE and low density polyethylene (LDPE) are typically used in film manufacturing. In processing of LLDPE films, difficulties arising due to the higher torque and extrusion pressure in comparison with LDPE films have been reported.[1] This was regarded to be due to the higher shear viscosity of LLDPE than that of LDPE.[2] But advantages in manufacturing process and also final properties of LLDPE film make it a polymer of choice. A few papers have been published on preparing PE-clay films.[3–5] Also, number of studies have used compatibilizers including maleated PE[6–12] and oxidized PE[13] to achieve exfoliated structures. Results of the above mentioned studies showed that the exfoliated structure can be achieved at low clay loadings only. Zhang et al. reported an exfoliated structure in LLDPE nanocomposite containing 2 wt % clay and 15 wt % of maleated PE.[6] Rheological properties of these nanocomposites were slightly affected, however, the presence of compatibilizer improved their ductility.[6] Wang et al. reported the presence of exfoliated structures in maleated PE nanocomposites containing 3 vol % of clay.[9] Durmus et al. used the oxidized PE as a new type of compatiblizer to prepare LLDPE nanocomposites showing that nanocomposites containing 5 phr of clay exhibited a lower gas permeability in comparison with those containing maleic anhydride.[11] The addition of fillers to polymers provides enhancements of their properties. Among these fillers clay minerals have been used as performance enhancing fillers. Clay minerals consist of layers of a few nanometers thick and hundreds nanometers long. The high aspect ratio of these layers is expected to provide enhanced properties. Thus, over the last two decades, it was reported that if these fillers are dispersed in nanometer scale in polymers, rather than in micrometer scales, better properties can be achieved. Polymer/layered silicate

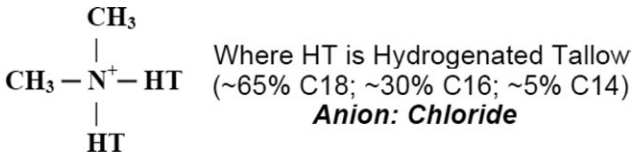

Figure 1. The structure of Cloisite® 20A.

nanocomposites have generated a great interest in industry and academia due to their improved properties, such as mechanical properties, thermal stability, and heat distortion temperature, flame retardancy, solvent resistance, chemical resistance, electrical conductivity, barrier properties, and optical clarity.[14–21] One of the main challenges in preparing polymer/clay nanocomposites is to achieve intercalation and preferably exfoliation, or delamination, of clay platelets. Because clay generally exists as stacks or tactoids, it requires a combination of high shear and surface modification to get intercalation and exfoliation. The exfoliation of clay is very important, since it dictates the final properties of nanocomposite. Current techniques for clay exfoliation rely on high shear mixing using extrusion equipment. However, this will only facilitate a partial exfoliation at best. Recently, ultrasonic waves were used to exfoliate nanoclays, causing high-energy mixing and dispersion due to acoustic cavitation: the formation, growth and implosive collapse of bubbles in a melt. Ultrasonic waves act as a mixing element analogous to kneading blocks in a twin-screw extruder, causing compression and expansion motions. These high intensity effects cause the clay agglomerates to separate into individual platelets and lead to partial exfoliation in PP/clay and HDPE/clay nanocomposites and full exfoliation in PA6/Clay nanocomposites.[22–25] Ultrasonic waves also breakdown the molecular chains reducing viscosity of the melt. In turn, the reduced viscosity facilitates dispersion of the exfoliated clay platelets throughout the matrix. The breakage of the polymer chains may also generates free radicals[26] that can interact with the clay platelets leading to intercalation and subsequent exfoliation of the clay.

A few studies on the effect of ultrasound on pure LLDPE were reported.[27–30] In particular, they showed that an ultrasonically aided single screw extrusion improved processing of LLDPE by reducing the die pressure and melt viscosity. Also, suppression of the sharkskin phenomenon on LLDPE extrudates was achieved[27] along with breakup of the dispersed phase of polyolefin elastomer (POE) in metallocene catalyzed LLDPE/POE blend.[28] Ultrasonically aided extrusion also led to an improvement of the elongation at break of LDPE/LLDPE blends.[29] An addition of the diatomite/polyethylene glycol mixture to LLDPE led to an increase of the critical shear rate for the onset of sharkskin fracture and, in the presence of ultrasonic treatment, an improvement of the processibility of the LLDPE mixture was reported.[30]

To the best of our knowledge there is no report on the effect of ultrasound on the preparation of LLDPE/clay nanocomposites and their film casting. The objectives of this work are: (1) to design a new ultrasonically aided extrusion film casting setup; (2) to manufacture LLDPE/clay nanocomposites cast films using this setup at the clay loadings up to 10 wt %; (3) to study the effect of ultrasonic treatments and clay loading on thermal, rheological, morphological, and mechanical properties and gas permeability of films.

EXPERIMENTAL

Materials and Methods

LLDPE with improved thermal stability made by the Dow Chemical Company under trade name DOWLEX™ 2056 G was used. The density and melt flow index (MFI) was 0.92 g cm^{-3} (ASTM D792) and 1 g/10 min (ASTM D1238). Cloisite® 20A is natural montmorillonite, modified with quaternary ammonium salts, was supplied by the Southern Clay Products. The chemical structure and properties and size of Cloisite® 20A are shown in Figure 1 and Table I, respectively. Cloisite® 20A was in the powder shape with 10% of the particles being <2 μ, 50% <6 μ and 90% <13 μ.

Cast films of LLDPE, 97.5/2.5, 95/5, 92.5/7.5, and 90/10 LLDPE/clay 20A nanocomposites were prepared in the ultrasonic single screw compounding extruder with a modified screw[31] connected to the cast film machine (Chill Roll Model, Killion Extruders, Cedar Grove, NJ). A schematic of this machine is shown in Figure 2. The screw has a diameter of 25.4 mm (1 in.) in the original extruder section, and then increases to 38.1 mm (1.5 in.) and then decreases to a 33 mm (1.3 in.) diameter shaft in the ultrasonic section to provide the 2.54 mm (0.1 in.) maximum gap for ultrasonic treatment. The diameter of the final section of the screw is 25.4 mm (1 in.). There were two mixing sections before the ultrasonic treatment zone: a 5.38-cm long union carbide mixer (UCM) and a 6.35-cm long melt star mixer (MSM). A data acquisition system (DI-715-U, Dataq Instruments, Akron, OH) was used to record pressure, temperature and ultrasonic power consumption. The ultrasonic system was composed of two identical sets of 20 kHz power supplies of 6 kW power capacity (2000bdc, Branson, Danbury, CT), fan cooled ultrasonic converters (Branson H.P. 101-135-124), 1 : 1 titanium boosters (Branson 101-149-096) and aluminum ultrasonic horns of 2.54 $\times$ 2.54 cm^2 cross section. The horns had tips with a radius of curvature of 18.4 mm. Both horns were operated simultaneously. Streamlined relieves on the sides of the barrel in the ultrasonic treatment area guided the polymer melt to flow equally through the two channels of 2.54 mm (0.1 in.) thickness between the ultrasonic horns and the rotating shaft. The ultrasonic horns were cooled with water to prevent overheating of the ultrasonic system. Water flow rate was controlled with 2500 cm^3 min^{-1} capacity flow meter (Key Instruments, Trevose, PA). The temperature of both horns was regulated at 80°C using an external temperature controller unit

Table I. Typical Properties of Cloisite® 20A

Treatment/ properties	Organic modifier[a]	Modifier concentration	% Moisture	% Weight loss on ignition
Cloisite® 20A	2M2HT	95 meq/100 g clay	<2%	38%

[a]MT2EtOH: methyl, tallow, bis-2-hydroxyethyl, quaternary ammonium.

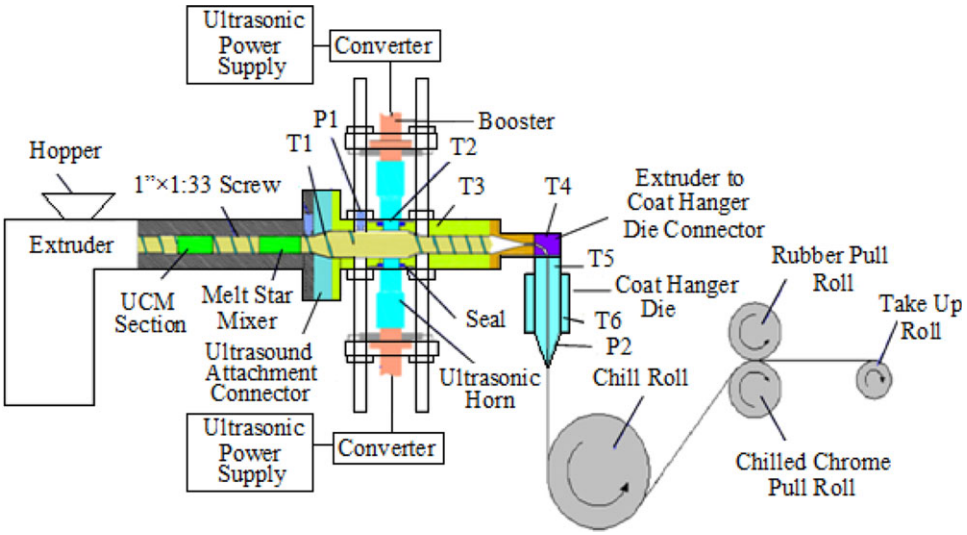

Figure 2. A schematic drawing of the online ultrasonic film casting. [Color figure can be viewed in the online issue, which is available at wileyonlinelibrary.com.]

(Neslab- RTE-110, Advanced Test Equipment, San Diego, CA). The take up section had a 20.32 cm (8 in.) diameter by 25.4 cm (10 in.) wide chrome plated cored chill roll and a 12.7 cm (5 in.) diameter by 25.4 cm (10 in.) wide pull rolls. The temperature of rolls was controlled using external temperature units (Sterl Tronic, Sterlco, New Berlin, WI) at 80°C. The coat hanger die was connected to the extruder with a specially designed connecting element. The die exit had a width of 17.78 cm (7 in.) with an adjustable thickness. A 1.85 mm (0.07 in.) thickness was used to prepare films. The film exiting the die passed a distance of 75 mm (2.95 in.) in air before touching the chill roll. Then the film was squeezed between two pull rolls and collected by a take up roll. Three different take up speeds of 91.44, 182.88, and 274.32 cm min^{-1} (3, 6, and 9 ft min^{-1}) were used to obtain films of different thicknesses. All the films were transparent. The thickness of the cast films of LLDPE and 90/10 LLDPE/clay nanocomposites obtained at different ultrasonic amplitudes as a function of draw down ratio (DDR) are shown in Figure 3. DDR was calculated as a ratio of the die thickness of die to the cast film thickness. As seen from Figure 3, the thickness of the cast films was in the range of 65–270 μm. The horns supplied ultrasonic waves at a frequency of 20 kHz and amplitudes of 5, 7.5, and 10 μm. A screw speed of 100 rpm and temperatures of 120 and 150°C for the feeding section and other zones, respectively, were utilized. The material was ultrasonically treated in the molten state at a flow rate of 0.50 g s^{-1}. The physical mixture of LLDPE pellets and clay powder in the required proportion was fed to the extruder using a feeder (K2v-T20 manufactured by K-Tron Soder). The extruder was operated under starved conditions.

Measurements of Properties

Thermal analysis was carried out using a differential scanning calorimeter (DSC) (Model DSC 7) manufactured by Perkin-Elmer and a TA Q 2000 DSC manufactured by Thermal Advantage Instrument Control. The operation temperature range was from 20 to 200°C. The heating and cooling rate was set to 10°C min^{-1}. Second heating was performed to remove the thermal history remaining in the material. The degree of crystallinity, X (%), was determined as $X(\%) = \Delta H/\Delta H_m$ where ΔH is the heat of fusion or crystallization of the polymer, ΔH_m is the enthalpy corresponding to the melting of a 100% crystalline polymer. ΔH_m was taken as 276.7 J g^{-1} for LLDPE.[32]

The complex dynamic shear viscosity, η^*, storage, G', and loss, G'', moduli and tan δ were measured in a rotational rheometer (Advanced Rheometric Expansion System, ARES) with a parallel plate geometry. The sample having a diameter of 25 mm, a thickness of 2 mm was used. The strain amplitude, frequency range, and temperature were set to 2%, 0.01–100 rad s^{-1}, and 150°C, respectively. ARES samples were prepared using a mini jet injection molding machine (DSM Research Micro Injection Molding Machine). A barrel temperature of 150°C, a mold temperature of 80°C, an injection pressure of 8 bar, a holding time of 10 s were used. The cast films were folded and fed into the barrel.

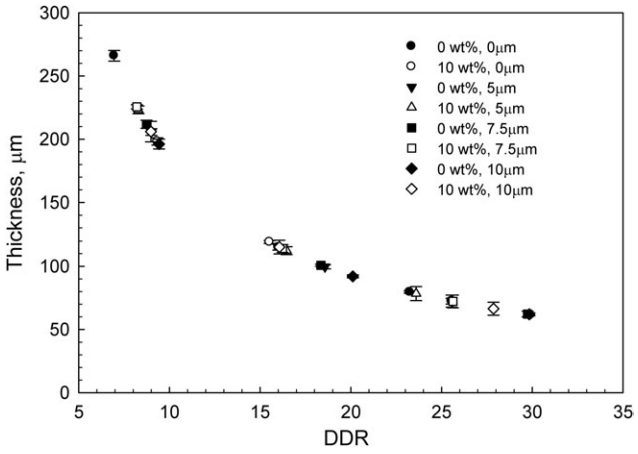

Figure 3. Thickness of cast films of LLDPE (filled symbols) and 90/10 LLDPE/clay nanocomposites (open symbols) at different ultrasonic amplitudes as a function of DDR.

Instron 5567 tensile tester was used to determine the stress–strain behavior of films. The Young's modulus, elongation, yield stress, yield strain, and toughness of materials were measured without using an extensometer. The cross-head speed of 100 mm min^{-1} and a load cell of 0.1 kN was used. Strips in the machine and transverse directions of cast films with a length of 50 mm, and a width of 12.5 mm were cut from cast films prepared at different clay loadings, ultrasonic amplitudes, and take up speeds.

Oxygen permeability of the films was measured using an oxygen permeation analyzer (Illinois Instrument, Model 8001, Johnsburg, IL). All sample films were cut into a circular shape of 10 cm diameter. Measurements were carried out in the presence of nitrogen gas with a purge rate of 1 unit. Permeability in OTR units of cm^3/m^2/day was measured and converted into units of cm^3 mm/m^2/day.

^{13}C NMR solid-state measurement was performed on a Bruker Avance III 300 for LLDPE cast films according to the procedures given in Refs. 33 and 34. The high temperature MAS probe was used. The material was packed into the MAS rotors and secured with a high temperature BN cap. The rotors were bathed in N_2 bearing gas to prevent the oxidative degradation and radical combination. Direct heating of the bearing gas provided a temperature stability of $\pm 0.1°C$ during MAS. Chemical shift values were calibrated using adamantane at room temperature. The 90° pulse lengths were set at 6.25 μm determined directly on the LLDPE melts under measurements. The temperature was set at 130°C.

A high resolution field emission scanning electron microscope (JSM-7401 F, JOEL, Peabody, MA) was used to observe aggregates of clay 20A in LLDPE. Also, adhesion of polymer to the clay surfaces was checked. In addition, a transmission electron microscopy and X-ray diffraction patterns were used to verify the complete dispersion and morphological structures (intercalated or exfoliated) of nanocomposites.

X-ray diffraction patterns of clay 20A, and cast films were obtained using a general area detector diffraction system (GADDS) by Bruker AXS. It is equipped with Bruker AXS HI-STAR 2D area detector and Cu Kα radiation of a wavelength of $\lambda = 1.54$Å and an operation voltage of 40 KV and a current of 40 mA. A stack of film of a total thickness of 3–5 mm was used in X-ray measurements. The stack of films was placed in the sample holder and analyzed within an exposure time of 2 min. The scanning range was from $2\theta = 2°$ to 32° with an increment of 0.1° in transmission mode.

A transmission electron microscope (TEM, TECNAI12, Philips) operating at 120 kV was used to study the morphology of nanocomposites. Special sample preparation was applied for films. A very thin slice of films were cut using a razor and put in a special curing case in a way that no wrapping or twisting of the slice can happen. Curing mixture composed of 23.8 mL of epoxy resin, 16.0 mL of dodecenyl succinic anhydride (DDSA), 14.3 mL methyl-5-norbornene-2,3-dicarboxylic anhydride (NMA), and 0.8 mL of benzyldimethylamine (BDMA) (2.5–3%) as an accelerator was prepared under the hood. Then three to five drops of curing mixture was added to the case. The case was moved to the vacuum oven and left for 24 h at 60°C for curing. All the materials were supplied by TED PELLA, Redding, CA. Then, a Reichert Ultracut low-temperature sectioning system was used to cut ultrathin specimens. Finally, the specimens were transferred into a copper grid.

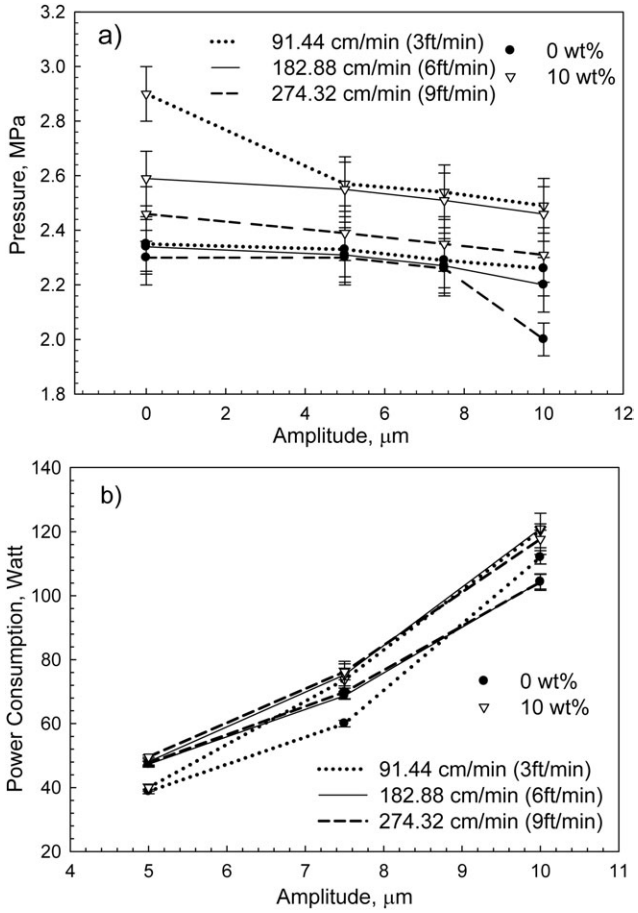

Figure 4. Pressure at the entrance of ultrasonic zone (a) and ultrasonic power consumption (b) as a function of ultrasonic amplitude of cast film of LLDPE and 90/10 LLDPE/clay nanocomposites at different take up speeds.

RESULTS AND DISCUSSION

Process Characteristics

The pressure at the entrance to ultrasonic treatment zone and ultrasonic power consumption as a function of ultrasonic amplitude during casting of films of LLDPE and 90/10 LLDPE/clay nanocomposites at different take up speeds are presented in Figure 4(a,b), respectively. It is observed that the pressure [Figure 4(a)] slightly decreased with application of ultrasound and decreases further with an increase of amplitude. This may be due to the reduction of friction between the melt and the surface of horn tips due to the ultrasonic vibration.[35] It is also due to a permanent change in the melt viscosity due to the presence of the clay causing enhanced cavitations.[22] Pressure during film casting of 90/10 LLDPE/clay nanocomposites is higher than that of LLDPE cast films due to the higher melt viscosity caused by an addition of clay. A lower pressure is seen

Table II. Melting Temperature, Crystallization Temperature, and Crystallinity for Untreated and Ultrasonically Treated Cast Films of LLDPE and 90/10 LLDPE/Clay Nanocomposites Prepared at a Different Take-up Speed

Clay loadings (wt %)	Take up speed (cm min^{-1})	Ultrasonic amplitude (μm)	Melting temperature (°C)	Crystallization temperature (°C)	Crystallinity (%)
0	91.44	0	111.2	97.1	40.5
		5	112.1	96.3	43.9
		7.5	111.6	96.8	47.2
		10	111.5	97.1	41.1
	182.88	0	111.5	96.9	44.6
		5	111.6	96.6	47.2
		7.5	111.4	97.2	50.1
		10	111.3	97.1	49.6
	274.32	0	111.4	96.9	44.6
		5	111.3	96.9	49.0
		7.5	111.4	96.9	50.9
		10	111.1	97.2	50.0
10	91.44	0	110.8	96.6	52.2
		5	111.1	96.7	51.8
		7.5	111.6	95.8	51.4
		10	111.2	96.2	48.9
	182.8	0	112.0	95.6	53.0
		5	111.5	96.1	51.1
		7.5	111.4	96.3	50.5
		10	111.4	96.2	48.4
	274.32	0	111.2	96.8	52.6
		5	111.7	96.1	51.3
		7.5	111.6	95.8	51.3
		10	111.0	96.7	49.7

with increasing take up speeds. This is due to additional tensile stresses generated in the melt by the elongational flow arising from the take up velocity, decreasing the resistance of the melt to flow through the die. The ultrasonic power consumption [Figure 4(b)] slightly increased with clay loading and increased tremendously with ultrasonic amplitude. The ultrasonic power consumption is due to the propagation of ultrasonic waves in material and dissipation of energy transferred to heat and power utilized to disperse clay filler and promote polymer chains penetration into clay galleries leading to an intercalated or exfoliated structure. Power consumption generally shows a slight increase with increasing take up speed. However, the reason for these slight changes in power consumption is presently unclear.

Thermal Properties

Melting and crystallization temperatures, and crystallinity of the untreated and ultrasonically treated cast films of LLDPE and 90/10 LLDPE/clay nanocomposites prepared at different take up speeds are listed in Table II. It can be seen that the melting and crystallization temperatures do not change with an addition of clay and ultrasonic treatment. However, crystallinity of LLDPE cast films obtained at all the take up speeds shows a maximum at an ultrasonic treatment at 7.5 μm, while crystallinity of cast films of 90/10 LLDPE nanocomposites decreases with ultrasonic amplitude due to a reduced mobility of polymer chains, as discussed later. The crystallinity of LLDPE cast films increased with increasing take up speeds due to the more stress induced orientation. Also, an increase in crystallinity of HDPE moldings with clay loading is observed, as reported in Ref. 36. It can be attributed to the fact that the clay may play a role of a nucleating agent.

Rheological Properties

Figure 5 illustrates the complex viscosity (a), storage (b) and loss (c) moduli and tan δ (d) as a function of frequency and the Cole–Cole plot (e) of molten cast films of the untreated and ultrasonically treated LLDPE and 90/10 LLDPE/clay nanocomposites prepared at 91.44 cm min^{-1} (3 ft min^{-1}) at different ultrasonic amplitudes. The complex viscosity of LLDPE at low frequencies increased, while at high frequencies slightly decreased at an amplitude of 10 μm [Figure 5(a)]. This is apparently due to the changes of the molecular structure of LLDPE under high amplitude of ultrasonic treatments as supported by the NMR studies, indicating the presence of additional branching under ultrasonic treatment of LLDPE, as discussed later. The complex viscosity significantly increased with an addition of clay and also with ultrasonic treatment at an amplitude of 10 μm. The observed increase of the complex viscosity of

Applied Polymer SCIENCE

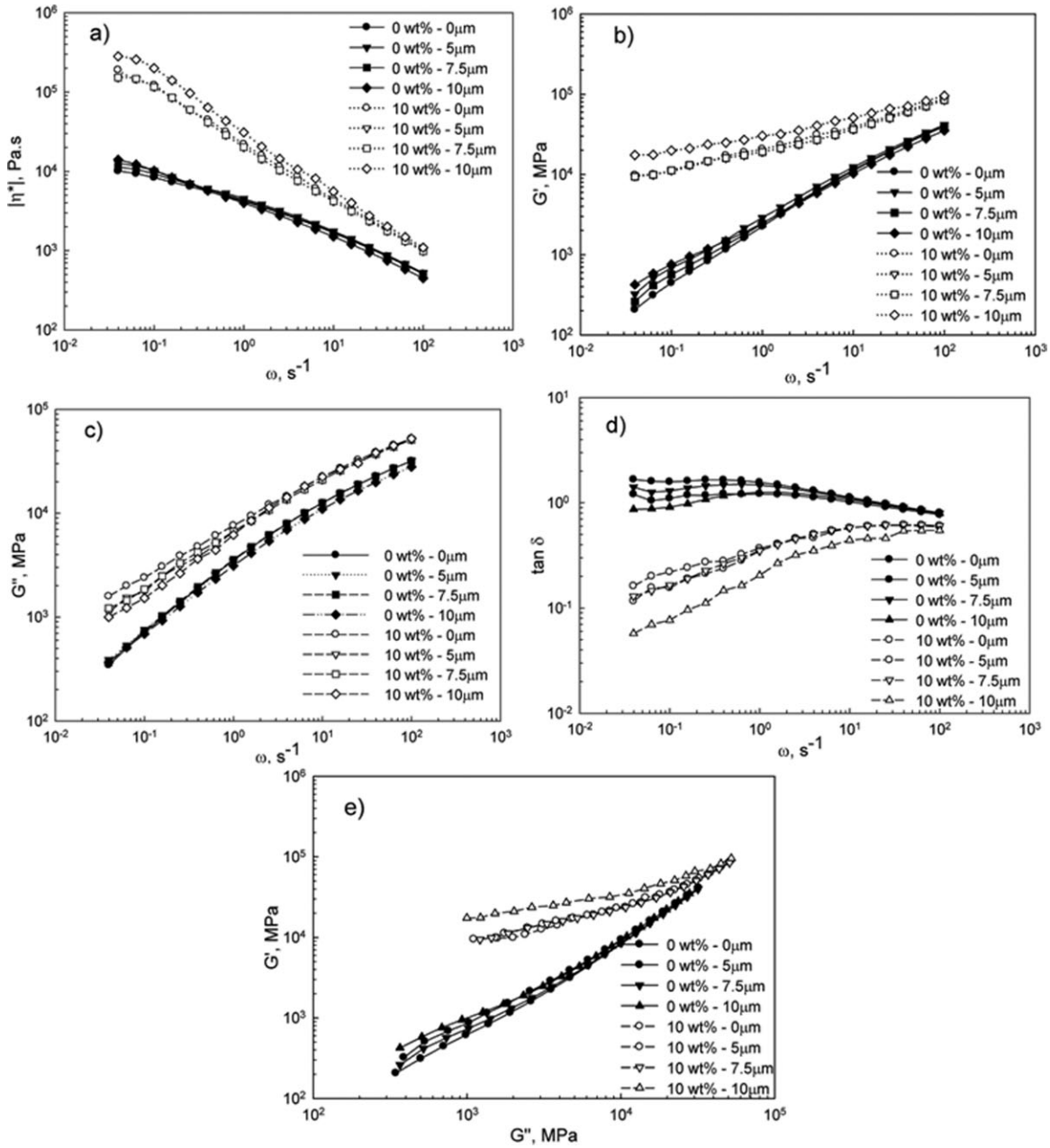

Figure 5. Complex viscosity (a), storage (b), loss (c) moduli, tan δ (d), and Cole–Cole plot (e) of melts of cast films of LLDPE and 90/10 LLDPE/clay prepared at take up speed of 91.44 cm min^{-1} (3 ft min^{-1}) untreated and treated at different ultrasonic amplitudes.

nanocomposites with ultrasonic amplitude was attributed to the nanoscale dispersion of the clay within the polymeric matrix. The latter improved the compatibility between the polymer matrix and layered silicates, so their viscosity increased. This finding is in agreement with that reported earlier for HDPE/clay nanocomposites.[22]

The storage, G', and loss, G'', moduli are shown in Figure 5(b,c). G' and G'' increased with an increase of frequency and clay loading. With increasing of ultrasonic amplitude, G' increases appreciably while G'' shows a decrease in molten cast films of nanocomposites. This increase in G' is more obvious in the case of cast films of 90/10 LLDPE/clay nanocomposites treated at an amplitude of 10 μm. Tan δ of LLDPE cast films increased with frequency, while tan δ of 90/10 LLDPE/clay nanocomposites show a plateau then a decrease in the value. Tan δ of LLDPE and 90/10 LLDPE/clay nanocomposites decreased with ultrasonic amplitude. The dependence of the storage modulus on the loss modulus (Cole–Cole plot) for cast films of untreated and ultrasonically treated LLDPE and 90/10 LLDPE/clay nanocomposites [Figure 5(e)] indicates that the G' vs. G'' functions for untreated and ultrasonically treated 90/10 LLDPE/Clay 20A nanocomposites significantly deviate from the functions for LLDPE. Such a deviation is an indication of the occurrence of some structural changes in these materials. In

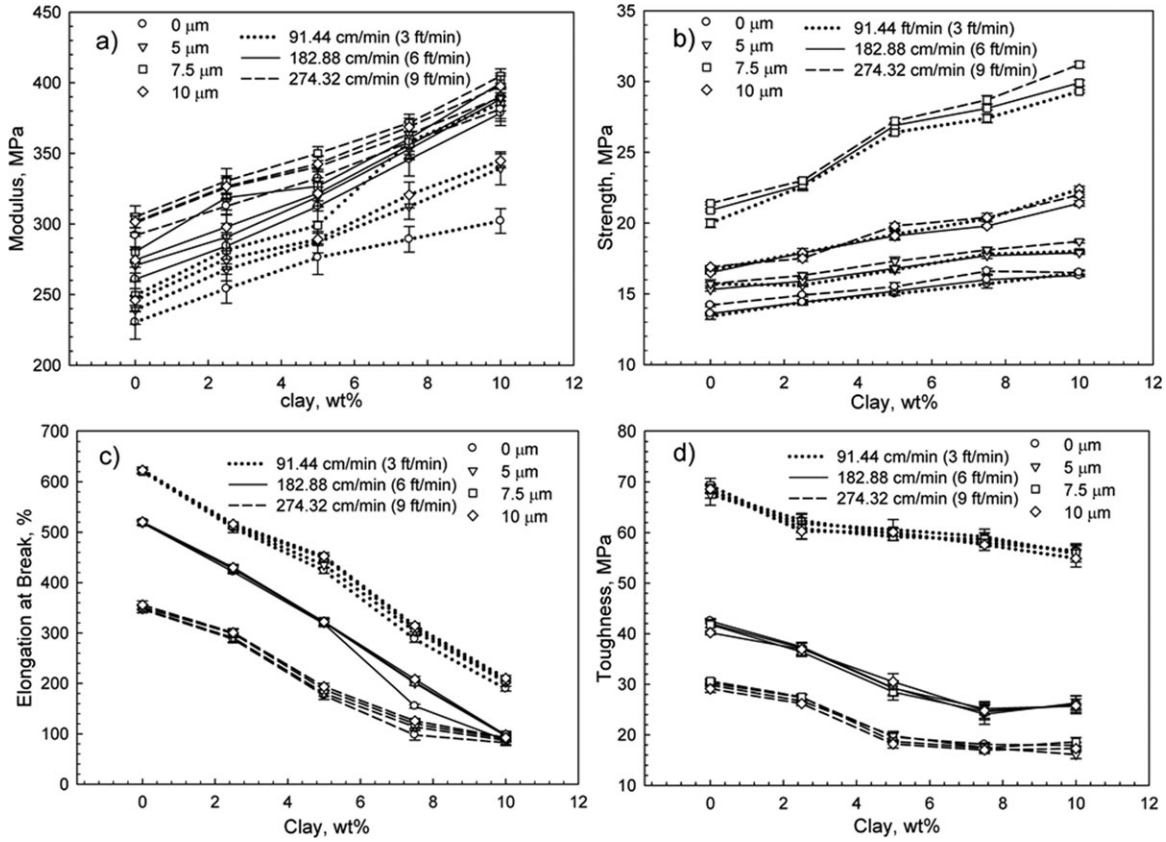

Figure 6. Young's modulus (a), strength (b), elongation at break (c), and toughness (d) of untreated and ultrasonically treated cast films of LLDPE and LLDPE/clay nanocomposites in the machine direction as a function of clay loadings, at various ultrasonic amplitudes and take up speeds.

fact, as shown later, an increase in LLDPE branching due to ultrasonic treatment takes place. An increase in complex viscosity and the storage modulus and a reduction in tanδ are caused by a better interaction between clay and LLDPE matrix. This can be a result of improved compatibilization effect due to ultrasonic treatment of LLDPE/clay nanocomposites leading to a reduction in the mobility of polymer chains. Evidently, due to this mobility reduction, a reduction in crystallinity occurred as was shown in Table II for all three take up speeds. Because of better compatibilization, an intercalated structure and better mechanical properties is expected, as will be shown below.

Mechanical Properties

Figures 6 and 7 show the mechanical properties, including the Young's modulus (a), strength (b), elongation at break (c), and toughness (d) of untreated and ultrasonically treated cast films of LLDPE and LLDPE/clay nanocomposites as a function of clay loadings at various ultrasonic amplitudes and take up speeds in the machine and transverse directions, respectively. For a more clear representation of the effect of take up speed on mechanical properties, Figure 8 shows the Young's modulus (a, b), strength (c, d), elongation at break (e, f), and toughness (g, h) as a function of the take up speed for untreated and ultrasonically treated LLDPE and 92.5/7.5 LLDPE/clay cast films in the machine and transverse directions. The Young's modulus was determined from the initial slope of the stress-strain curves within the range of strains from 0 to 0.05. As seen from Figures 6(a) and 7(a), the Young's modulus in both the machine and transverse directions increased with clay loadings. The Young modulus shows the highest value at an amplitude of 7.5 μm in both the machine and transverse directions. The Young's modulus in the both machine and transverse directions increased with increasing take up speeds [Figures 6(a), 7(a), and 8(a,b)] possibly due to the increase of crystallinity as given in Table II. The strength in the machine direction [Figure 6(b)] increased with increasing clay loadings, while the strength in the transverse direction showed a maximum at 7.5 wt % and then significantly drops at 10 wt % [Figure 7(b)]. The strength of cast films treated at an ultrasonic amplitude of 7.5 μm was the highest in both the machine and the transverse directions. There are almost no changes in the strength values in the machine directions due to the changes in the take up speeds. However, a slight increase in the strength of LLDPE cast films and a slight decrease in the strength of untreated 92.5/7.5 LLDPE/clay cast films in the transverse direction is seen in Figure 8(d) with increasing take up speed. Figure 6(c) shows that the elongation at break in the machine direction decreased with increasing both clay loadings and take up speeds. Ultrasonic treatment slightly increases the elongation at break in the machine direction. Figure 7(c) shows that the effect of clay loadings and ultrasonic treatment on the elongation at break in the transverse direction is the same as in the machine direction. However, in the transverse direction the elongation at break of cast films of untreated and ultrasonically treated nanocomposites containing

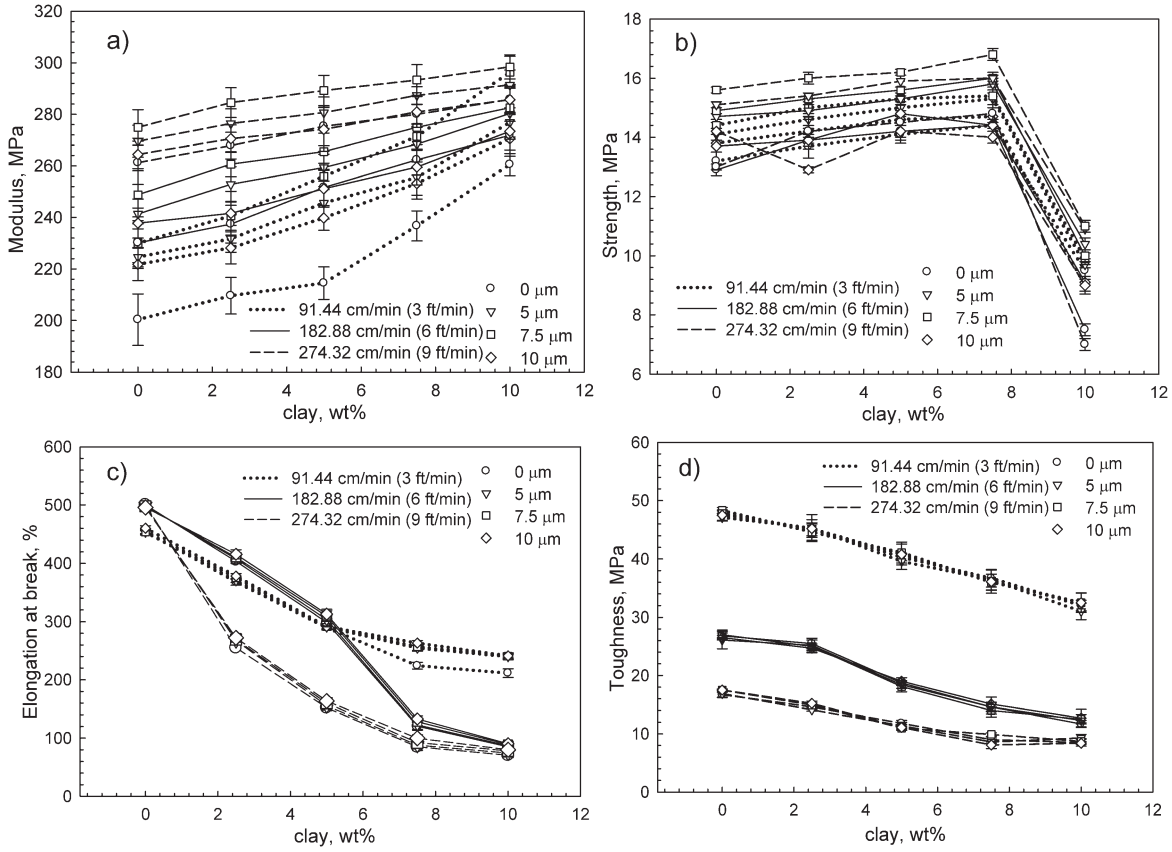

Figure 7. Young's modulus (a), strength (b), elongation at break (c), and toughness (d) of untreated and ultrasonically treated cast films of LLDPE and LLDPE/clay nanocomposites in the transverse direction as a function of clay loadings, at various ultrasonic amplitudes and take up speeds.

7.5 and 10 wt % of clay decreased with increasing take up speeds. At lower concentrations the highest value of the elongation at break was at a take up speed of 182.88 cm min^{-1} (6 ft min^{-1}) [Figure 7(c)]. LLDPE cast films prepared at 182.88 and 274.32 cm min^{-1} (6 and 9 ft min^{-1}) showed almost the same elongation at break [Figure 8(f)]. Figures 6(d), 7(d), and 8(g,h) show that the toughness of cast films decreased with increasing clay loadings and take up speeds in both the machine and transverse directions. These figures also show almost no effect of ultrasonic treatment on the toughness values in both the machine and transverse directions. Finally, it should be noted that all mechanical properties of films in the machine direction were higher than those in the transverse direction. From the mechanical properties, it can be concluded that ultrasonic treatment evidently played an important role in the dispersion of clay in LLDPE matrix by creating strong interfacial adhesion of clay with the matrix.

Oxygen Permeability Properties

Figure 9 shows the oxygen permeability of cast films of LLDPE and LLDPE/clay nanocomposites as a function of clay loadings at various ultrasonic amplitudes and at a take up speed of 91.44 (a), 182.88 (b), and 274.32 (c) cm min^{-1}. The oxygen permeability of cast films decreased with increasing clay concentration due to the creation of a more tortuous path for oxygen molecules to diffuse through the film. As seen from Figure 9, the oxygen permeability of LLDPE and LLDPE/clay cast films show a decrease and then an increase with ultrasonic amplitude. The lowest oxygen permeability of these films was observed at an ultrasonic amplitude of 7.5 μm. This trend can be explained by comparison with crystallinity of LLDPE films in Table II. This table indicates that cast films prepared at an ultrasonic amplitude of 7.5 μm exhibited the highest crystallinity. In the case of cast films of nanocomposites, both the crystallinity and the presence of clay particles must be considered. As indicated in Table II, crystallinity of nanocomposites is higher than those of LLDPE cast films, therefore, their gas permeability showed a lower value. However, with increasing ultrasonic amplitude the crystallinity of nanocomposites decreased but the permeability of cast films of nanocomposites showed a minimum at an ultrasonic amplitude at 7.5 μm.This indicates that not only crystallinity will play a role in the oxygen permeability, but also other structural changes taking place under ultrasonic treatment. The oxygen permeability is also decreased with increasing take up speeds due to the higher crystallinity developed in the cast films, as seen in Table II.

Structural Properties

The data obtained by NMR spectroscopy of the untreated and ultrasonically treated cast films of LLDPE at 7.5 μm prepared at 91.44 cm min^{-1} (3 ft min^{-1}) are shown in Figure 10. The LLDPE structure as given in Refs. 33 and 34 is also shown in Figure 10. C^* and C^1 in this structure are presented by carbon in the middle of the backbone of repeated LLDPE unit and by

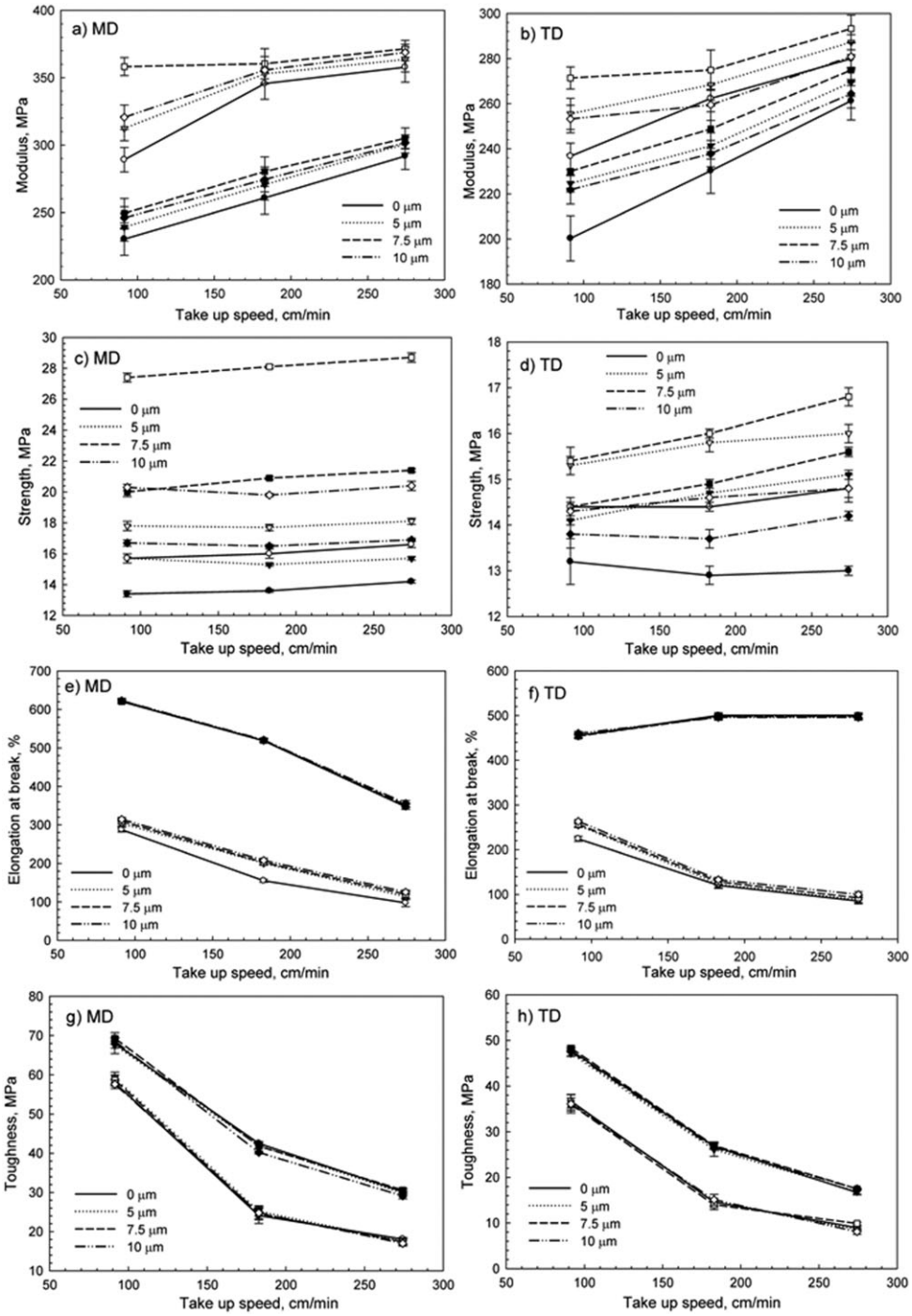

Figure 8. Young's modulus (a, b), strength (c,d), elongation at break (e,f), and toughness (g,h) of untreated and ultrasonically treated cast films of LLDPE (filled symbols) and 92.5/7.5 LLDPE/clay nanocomposites (open symbols) as a function of take up speeds.

end carbon in the branch. The LLDPE spectrum in Figure 10(a) indicates the presence of peaks at 30.31 and 14.43 ppm. These peaks are related to C^* and C^1, respectively. The ratio of the area under these two peaks in the untreated and treated samples would show if any branching was created by the action of the ultrasound. Software Topsin (Bruker) with fitting the Lorentz function was used to calculate the area under the peaks. The result reveals that for the untreated sample, the peak area of backbone middle carbon (C^* at 30.31 ppm)[33,34] is 15344873472.00. The end group[33,34] (C^1 at 14.43 ppm) is 153490016.00. The ratio of end group to the middle carbon is 0.0100027. For the treated sample, the middle carbon (C^* at 30.32 ppm) is 17374560256.00. End group (C^1 at 14.49 ppm) is 188339376.00. The ratio is 0.0108399. It indicates that the branching in LLDPE indeed occurred under ultrasonic treatment with an increase of the degree of branching roughly by 8%. Obviously, the observed branching occurs through degradation of macromolecular chains. However, further structural

Applied Polymer SCIENCE

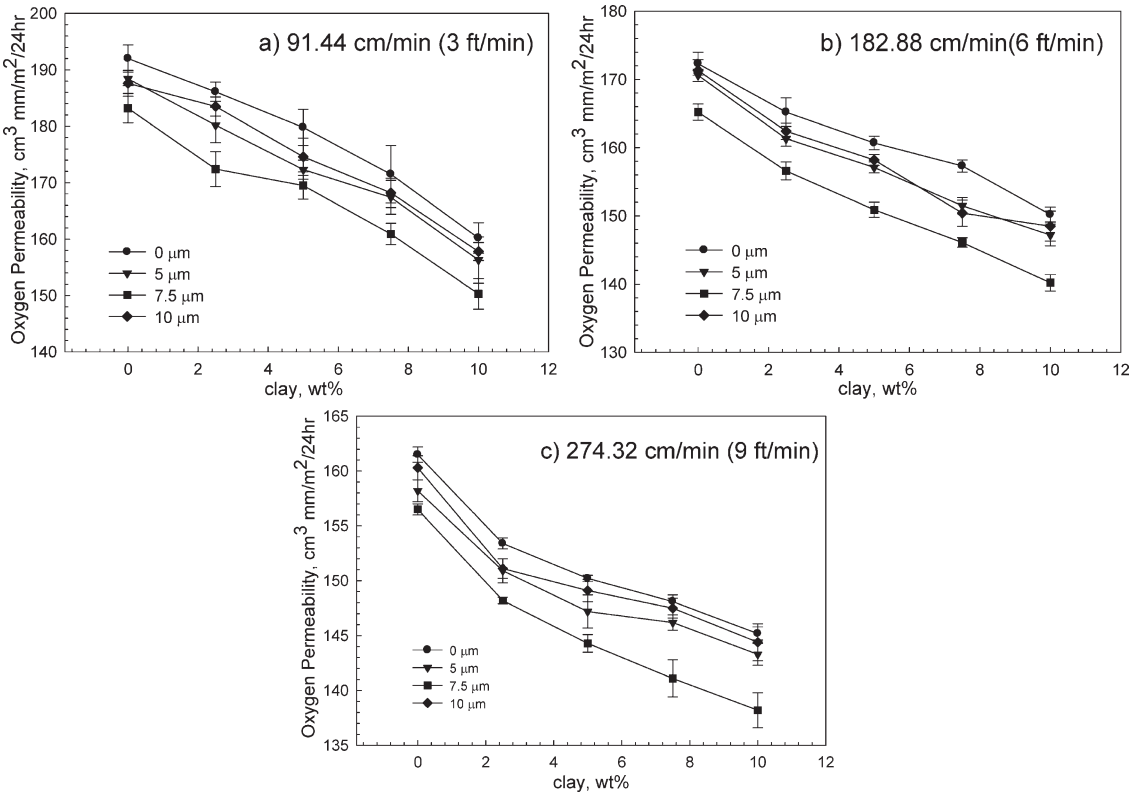

Figure 9. Oxygen permeability of cast films as a function of clay concentration at various ultrasonic amplitudes and a take up speed of 91.44 cm min^{-1} (a), 182.88 cm min^{-1} (b), and 274.32 cm min^{-1} (c).

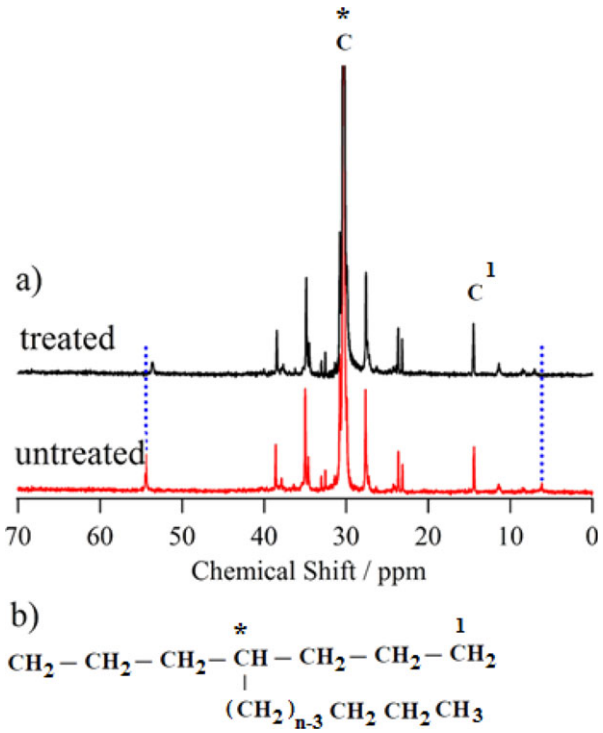

Figure 10. NMR spectra of untreated and ultrasonically treated LLDPE cast film at an amplitude of 7.5 μm prepared at 91.44 cm min^{-1} (3 ft min^{-1}) (a) and LLDPE branched structure according to[33,34] (b). [Color figure can be viewed in the online issue, which is available at wileyonlinelibrary.com.]

studies are required to fully understand the mechanism of processes taking place during ultrasonic treatment of LLDPE.

XRD patterns of clay 20A and cast films of nanocomposites obtained at various ultrasonic amplitudes and clay loadings in the range of 2θ varying from 2.0 to 10 degrees at a take up speed of 91.44 cm min^{-1} (3 ft min^{-1}) are shown in Figure 11. The organoclay shows a broad intensity peak at 2θ = 3.7°. As

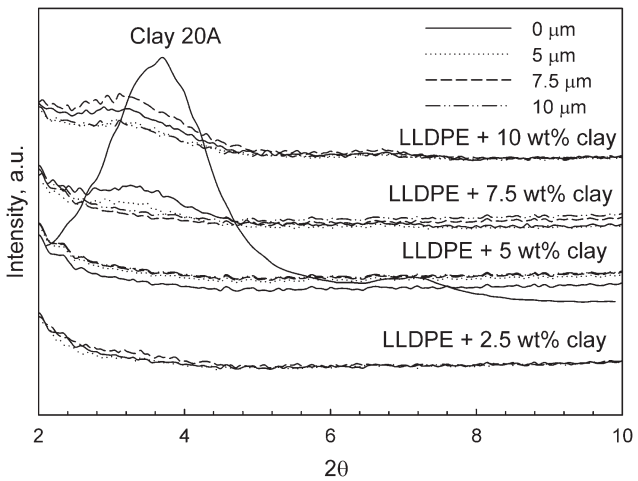

Figure 11. XRD patterns of clay 20A and cast films of LLDPE/clay films prepared without and with ultrasonic treatment at various clay loadings and amplitudes at a take up speed of 91.44 cm min^{-1} (3 ft min^{-1}).

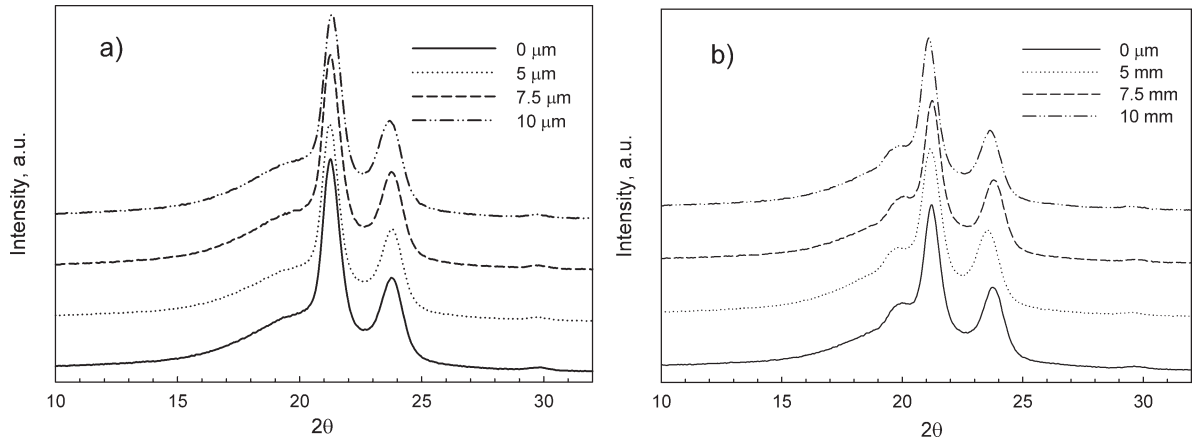

Figure 12. XRD patterns of LLDPE (a), and 90/10 LLDPE/clay 20A (b) cast films prepared without and with ultrasonic treatment of various amplitudes at a take up speed of 91.44 cm min^{-1} (3 ft min^{-1}).

seen from Figure 11, this peak is absent in cast films of untreated and ultrasonically treated 97.5/2.5 and 95/5 LLDPE/clay 20A nanocomposites, indicating their completely exfoliated structure. The X-ray pattern of untreated cast film of 92.5/7.5 LLDPE/clay nanocomposite show a peak corresponding to an arrangement of clay layers. However, upon application of ultrasound, this peak is disappeared. Based on these angles the interlayer distances were calculated by using Bragg's Law.[37] These distances are 2.38 nm for clay 20A and 3.24 nm for the cast films of untreated 92.5/7.5 LLDPE/clay nanocomposites. With an addition of 10 wt % of clay the peak corresponding to the clay is seen in the XRD patterns, but at lower angles corresponding to the higher interlayer distance indicating the intercalated structure. This observation may serve as an evidence that clay galleries are intercalated due to peeling apart of stacks of platelets. The combination of the ultrasonic treatment and high shear stresses imposed during melt mixing breaks up clay aggregates and separates platelet stacks allowing polymer chains to penetrate into the galleries. XRD patterns of cast films of untreated and ultrasonically treated LLDPE and 90/10 LLDPE/clay nanocomposites in the range of 2θ varying from 10 to 32 degrees are shown in Figure 12(a,b), respectively. It is observed

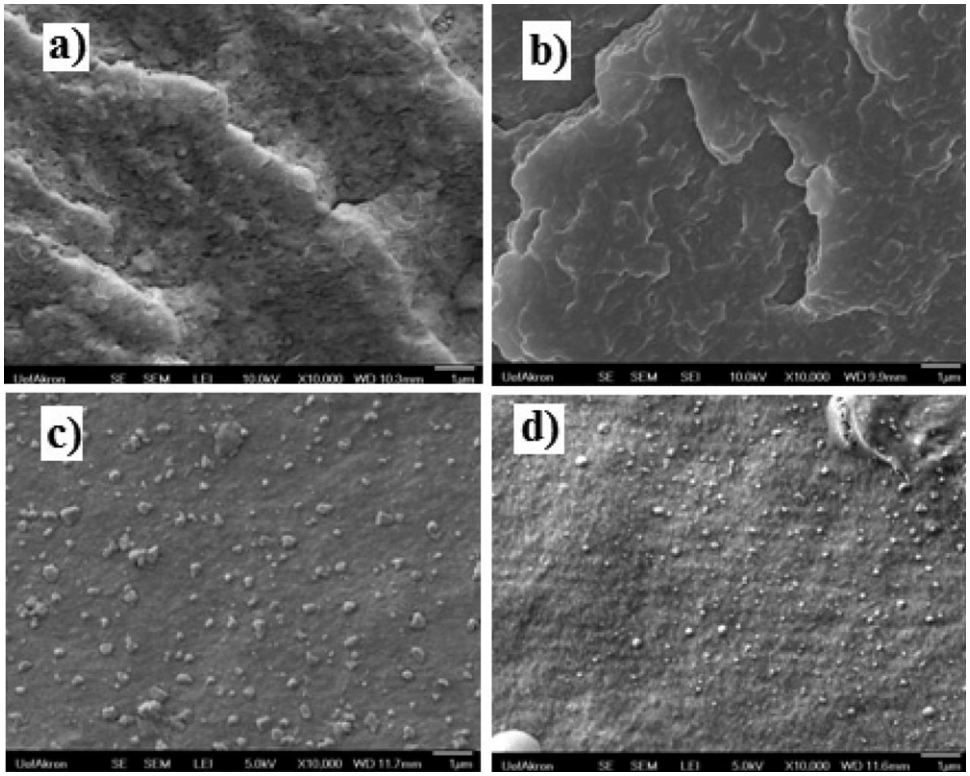

Figure 13. SEM images of cast films obtained at a take up speed of 91.44 cm min^{-1} (3 ft min^{-1}) of 92.5/7.5 (a,b) and 90/10 LLDPE/clay (c,d) of untreated (a,c) and ultrasonically treated at 10 μm (b,d).

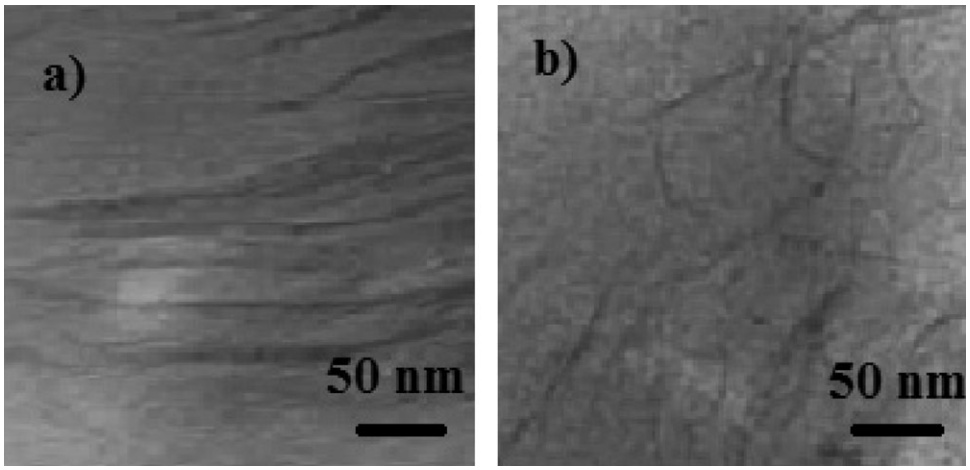

Figure 14. TEM images of untreated (a) and ultrasonically treated at 10 μm (b) of cast films of 92.5/7.5 of LLDPE/clay nanocomposites obtained at a take up speed of 91.44 cm min^{-1} (3 ft min^{-1}).

that X-ray diffraction patterns of LLDPE generally have three reflection peaks with the main reflections being at 2θ of 21.5 and 23.8 degrees and a shoulder with weak reflection at about 19.5 degree. These peaks and shoulder are similar to those reported for LLDPE by Bhadrakumari and Predeep.[38] The two main peaks arise from the crystalline regions and the shoulder arises from the amorphous region of LLDPE. Some small changes in the values of intensity and 2θ are observed at various ultrasonic amplitudes. The shoulder at 19.5 degrees is converted to a peak with increasing the clay loadings. At the same time the intensity of peaks at 2θ at 21.5 and 23.8 degrees decreased and the peaks slightly shifted to a lower angle.

The results concerning dispersion of clay obtained from the XRD studies were further supported by the SEM and TEM studies. SEM images of cast films of 92.5/7.5 and 90/10 LLDPE/clay nanocomposites of untreated and ultrasonically treated at an amplitude of 10 μm prepared at take up speed of 91.44 cm min^{-1} (3 ft min^{-1}) are shown in Figure 13. SEM images of untreated 92.5/7.5 LLDPE/clay nanocomposites [Figure 13(a)] show the presence of clay particles while with ultrasonic treatment at an amplitude of 10 μm [Figure 13(b)] the clay particles are absent. This is in agreement with the absence of peak corresponding to clay in XRD patterns (Figure 11). It is an indication of achieving of the exfoliated structure as also confirmed by the TEM images presented below. From the SEM images of cast films of 90/10 LLDPE/clay nanocomposites [Figure 13(c,d)], it is evident that with ultrasonic treatment at an amplitude of 10 μm, the clay particles were broken to smaller ones. Clearly, a better dispersion was achieved. The intercalated structure was observed in 90/10 LLDPE/clay films, as indicated by the SEM micrograph in Figure 13(d) and by the XRD patterns shown in Figure 11.

TEM images of cast films of 92.5/7.5 LLDPE/clay nanocomposites of untreated and ultrasonically treated at an amplitude of 10 μm at a take up speed of 91.44 cm min^{-1} (3 ft min^{-1}) are shown in Figure 14(a,b), respectively. An intercalated structure can be seen from TEM image in Figure 14(a) for the untreated sample. The exfoliated structure can be seen in Figure 14(b) for the ultrasonically treated samples. These evidences are in agreement with XRD patterns of Figure 11. This indicates that the polymer has indeed entered into the intergallery spacing where individual clay layers were being dispersed in the polymer matrix. This may be due to the complete exfoliation that occurred under ultrasonic treatment.

CONCLUSIONS

A continuous film casting process with the aid of ultrasound was developed to prepare films from polymer/clay nanocomposites. In this process, compounding, ultrasonic treatment and film casting were combined in a single step process. The significant dispersion and exfoliated structure in the cast films of LLDPE/clay nanocomposites up to 7.5 wt % with aid of ultrasonic treatment was obtained without use of a compatibilizer. Also, the intercalated structure was obtained in the cast films of 90/10 LLDPE/clay nanocomposites. The cast films were transparent, even at 10 wt % of clay loading. Effects of clay concentrations, ultrasonic amplitude, and take up speed were studied using different techniques. Rheological studies indirectly indicated improved compatibility between the polymer matrix and layered silicates under action of ultrasound. The studies revealed that ultrasonic treatment at an amplitude of 7.5 μm provides the highest crystallinity and mechanical properties and the lowest gas permeability. NMR studies were carried out showing an increase in branching of LLDPE with ultrasonic treatment.

ACKNOWLEDGMENTS

The authors are grateful for the financial support provided by Appleton Papers Inc. under contract W911QY-08-C-0085 with the US Army Natick Soldier Systems Center. The authors also wish to thank Professor Toshikazu Miyoshi and Ms. Jia Kang for providing NMR data.

REFERENCES

1. Cooke, D. L.; Koyich, M. *SPE ANTEC* **1991**, *37*, 206.
2. Ramamurthy, A. V. *Adv. Polym. Technol.* **1986**, *6*, 489.

3. Wang, K. H.; Koo, C. M.; Cung, I. J. *J. Appl. Polym. Sci.* **2003**, *89*, 2131.
4. Bafna, A.; Beaucage, G.; Mirabella, F.; Metha, S. *Polymer* **2003**, *44*, 1103.
5. Zhong, Y.; Janes, D.; Zheng, Y.; Hetzer, M.; Kee, D. D. *Polym. Eng. Sci.* **2007**, *47*, 1101.
6. Zhang, M.; Sundararaj, U. *Macromol. Mater. Eng.* **2006**, *291*, 697.
7. Stoeffler, K.; Lafleur, P. G.; Denault, J. *Polym. Eng. Sci.* **2008**, *48*, 1449.
8. Zhong, Y.; Janes, D.; Zheng, Y.; Hetzer, M.; De, K. D. *Polym. Eng. Sci.* **2007**, *47*, 1101.
9. Wang, K. H.; Choi, M. H.; Koo, C. M.; Xu, M.; Chung, I. J.; Jang, M. C. *J. Polym. Sci. B Polym. Phys.* **2002**, *40*, 1454.
10. Hotta, S.; Paul, D. R. *Polymer* **2004**, *45*, 7639.
11. Parija, S.; Nayak, S.; Jena, S. *Polym. Plast. Technol. Eng.* **2007**, *46*, 183.
12. Gopakumar, T. G.; Lee, J. A.; Kontopoulou, M.; Parent, J. S. *Polymer* **2002**, *43*, 5483.
13. Durmus, A.; Woo, M.; Kasgoz, A.; Macosko, C. W.; Tsapatsis, M. *Eur. Polym. J.* **2007**, *43*, 3737.
14. Alexandre, M.; Dubois, P. *Mater. Sci. Eng. Rep.* **2000**, *28*, 1.
15. Chen, C.; Curliss, D. *SAMPE J.* **2001**, *37*, 20.
16. Vaia, R. *AMPTIAC Q.*, **2002**, *6*, 17.
17. Jiang, L.; Wei, K. *J. Appl. Phys.* **2002**, *92*, 6219.
18. Kenig, S.; Ophir, O.; Shepelev, O.; Weiner, F. *ANTEC* **2002**, *1*, 794.
19. Wang, S.; Hu, Y.; Qu, Z.; Wang, Z.; Chen, Z.; Fan, W. *Mater. Lett.* **2003**, *57*, 2675.
20. Zhang, J.; Wilkie, C. *Polym. Degrad. Stab.* **2003**, *50*, 163.
21. Gopakumar, T. G.; Lee, J. A.; Parent, J. S. *Polymer* **2002**, *43*, 5483.
22. Swain, S. K.; Isayev, A. I. *Polymer* **2007**, *48*, 281.
23. Lapshin, S.; Isayev, A. I. *J. Vinyl Additive Technol.* **2007**, *13*, 40.
24. Swain, S. K.; Isayev, A. I. *J. Appl. Polym. Sci.* **2009**, *114*, 2378.
25. Lapshin, S.; Swain, S. K.; Isayev, A. I. *Polym. Eng. Sci.,* **2008**, *48*, 1584.
26. Basedow, A. M.; Ebert, K. *Adv. Polym. Sci.,* **1977**, *22*, 83.
27. Guo, S.; Li, Y.; Chen, G.; Li, H. *Polym. Int.* **2003**, *52*, 68.
28. Wu, H.; Bao, W.; Guo, S. *Polym. Eng. Sci.* **2010**, *50*, 2229.
29. Wu, H.; Guo, S.; Chen, G.; Shi, H. *J. Appl. Polym. Sci.* **2004**, *94*, 2522.
30. Chen, J.; Liu, X.; Li, H. *J. Appl. Polym. Sci.* **2007**, *103*, 1927.
31. Isayev, A. I.; Jung, C.; Gunes, K.; Kumar, R. *Intern. Polym. Process.* **2008**, *4*, 395.
32. France, C.; Hendra, P. J.; Maddams, W. F.; Willis, H. A. *Polymer* **1987**, *28*, 710.
33. Liu, W.; Rinaldi, P. L.; McIntosh, L. H.; Quirk, R. *Macromolecules* **2001**, *34*, 4757.
34. Pollard, M.; Klimke, K.; Graf, R.; Spiess, H. W.; Wilhelm, M.; Sperber, O.; Piel, C.; Kaminsky, W. *Macromolecules* **2004**, *37*, 813.
35. Tukachinsky, A.; Schworm, T.; Isayev, A. I. *Rubber Chem. Technol.,* **1996**, *103*, 69.
36. Deng, C.; Gao, X.; Chen, Z.; Xueb, S.; Shenb, K. *Polym. Intern.* **2010**, *59*, 1660.
37. Cullity, B. D.; Stock, S. R. Elements of X-ray Diffraction, 3rd ed.; Addison Wesley: Reading MA, **2001**.
38. Bhadrakumari, S.; Predeep, P. *Supercond. Sci. Technol.,* **2006**, *19*, 808.